THE ASTROPHYSICAL JOURNAL, 318:124–138, 1987 July 1

APERTURE SYNTHESIS OBSERVATIONS OF THE CIRCUMNUCLEAR RING IN THE GALACTIC CENTER

R. GÜSTEN,[1,2] R. GENZEL,[1] M. C. H. WRIGHT,[3] D. T. JAFFE,[1] J. STUTZKI,[1] AND A. I. HARRIS[1]
University of California, Berkeley
Received 1986 August 14; accepted 1986 December 10

ABSTRACT

We report 88 GHz aperture synthesis observations of HCN $J = 1 \rightarrow 0$ emission and absorption in the central 5 pc of the Galaxy and single-dish measurements of HCN $1 \rightarrow 0$ and CO $J = 7 \rightarrow 6$ line profiles at galactocentric radius $R = 5.5$ pc. The HCN synthesis data, taken at 5″–10″ spatial and 4 km s^{-1} spectral resolution with the Hat Creek millimeter wave–interferometer, show a highly inclined, clumpy ring of molecular gas surrounding the ionized central 2 pc of the Galaxy. The ring is the inner edge of a thin disk extending in the HCN aperture synthesis data to about 5 pc and to ≥ 7 pc in lower excitation lines.

The molecular gas is dynamically coupled to ionized gas in the central cavity. The "western arc" appears to be the ionized inner surface of the molecular ring. The "northern" and "eastern" arms and the "western bar" may be streamers of ionized gas falling from the ring toward the center.

The dominant large-scale velocity pattern of the majority of the molecular gas in the inner 5 pc is rotation. No overall radial motion greater than about 20–30 km s^{-1} is apparent. The rotation is perturbed in several ways. There is a very large local velocity dispersion throughout the disk. The disk shows changes in position angle with radius and in inclination with azimuthal angle (warps). A bright, redshifted cloud is located in the western part of the inner ring but does not participate in the rotation. These characteristics and the high degree of clumpiness indicate a nonequilibrium configuration of short ($\leq 10^4$–10^5 yr) dynamical lifetime.

The HCN velocity field southwest of Sgr A* gives approximately constant rotation velocities of about 110 km s^{-1} between 2 and 5 pc. Lower velocities (70–80 km s^{-1}) are indicated in the [C II] and CO $7 \rightarrow 6$ emission lines at $R \geq 4$ pc and higher velocities ($\sim$130–140 km s^{-1}) are indicated by the HCN data in the northern part of the ring at $R = 2$ pc.

The neutral gas ring may represent a circumnuclear accretion disk which feeds interstellar matter into the central parsec. The disk's turbulence may be maintained by dissipation of the rotational energy of the gas and by energy input from the center. The most likely explanation for the well-defined central cavity is a recent explosion in the Galactic center.

Subject headings: galaxies: nuclei — interstellar: molecules

I. INTRODUCTION

Becklin, Gatley, and Werner (1982) showed that the region within 2 pc of the Galactic center is largely devoid of interstellar matter and is surrounded by a dust ring. Lester *et al.* (1981) and Genzel *et al.* (1982, 1984, 1985), investigating neutral oxygen fine-structure line emission, and Liszt *et al.* (1983, 1985), investigating H I 21 cm and CO 2.6 mm lines, found that the ring consists mainly of neutral gas. The neutral gas velocities are indicative of rotation about the center with a rotation axis close to that of galactic rotation (Genzel *et al.* 1982). Genzel *et al.* (1985) and Harris *et al.* (1985) demonstrated that the neutral gas and dust ring is dense [$n(H_2) \approx 10^5$ cm^{-3}], warm ($T \approx$ 150–450 K), clumpy, and has a high local velocity dispersion. Gas pressure decreases with distance from the center. Gatley *et al.* (1984, 1986) found very hot ($T \approx 2000$ K) molecular hydrogen at the inner edge of the ring, presumably excited by shocks. In the framework of a rotating, axisymmetric equilibrium disk Lugten *et al.* (1986) and Harris *et al.* (1985) traced the rotation curve of the neutral gas and found that the rotation velocities fall by a factor of 1.5 to 2 between 2 and 7 pc, suggestive of a central mass concentration. Serabyn *et al.* (1986) and Lo (1986), on the other hand, investigating the CO $1 \rightarrow 0$ and $2 \rightarrow 1$ and CS $2 \rightarrow 1$ mm transitions between 3 and 7 pc, deduced approximately constant velocities.

New measurements at high spatial and spectral resolution could determine the small-scale structure and velocity field of the neutral gas and allow the study of the interaction between molecular gas and ionized gas at the inner edge of the disk. We report here aperture synthesis observations of the HCN $J = 1 \rightarrow 0$ transition with the Hat Creek millimeter wave–interferometer which probe the distribution and dynamics of dense molecular gas at 5″–10″ spatial resolution and 4 km s^{-1} spectral resolution. We also present measurements of the CO $J = 7 \rightarrow 6$ ($\lambda = 372$ μm) and HCN $1 \rightarrow 0$ line profiles at 110″ distance from the center, taken with single-dish telescopes at about 25″ resolution. In the following, we adopt for convenience 10 kpc as the distance of the Galactic center (20″ = 1 pc).

II. OBSERVATIONS

The HCN data were taken between 1985 November and 1986 March with the three-element interferometer of the Hat Creek Observatory (Welch and Thornton 1985). Measurements from configurations with three spacings each, with baselines up to $\sim$177 m north-south and $\sim$43 m east-west, were obtained for a full Galactic center period (5.5 hr) on each of two positions. Phase center position A was the nonthermal radio point source Sgr A* (R.A. = $17^h42^m29^s.3$, decl. =

[1] Department of Physics.
[2] On leave from the Max-Planck Institute for Radio Astronomy, Bonn.
[3] Radio Astronomy Laboratory, Department of Astronomy.

$-28°59'18''.6$ (1950); Brown, Johnston, and Lo 1981). Position B was at R.A. = $17^h42^m28^s.7$, decl. = $-29°0'17''.4$, shifted 1′ southeast along the approximate major axis of the disk toward the negative velocity emission lobe. The synthesized point source response had a FWHM of $10''.8 \times 9''$ (R.A. × decl.) for natural weighting of the data. The Fourier-transformed data were cleaned and restored with a Gaussian beam of the same FWHM. The Fourier-transformed data were also independently processed with uniform weighting and cleaning and with the maximum entropy method (MEM: Gull and Daniell 1978), resulting in angular resolutions of 5″–7″.

The instrumental phase was calibrated against the nearby extragalactic source NRAO 530. The flux density scale was established to an accuracy of $\pm 20\%$ from observations of Venus and Jupiter, with the brightness temperatures given by Ulich (1981). All three 6 m-antennas were equipped with cooled Schottky mixer receivers. Typical total system temperatures toward the low-elevation Galactic center sources were about 500 K. The 256 channel correlator was split into four spectrometers of 80 MHz bandwidth each, yielding a velocity resolution of 4.23 km s^{-1}. The spectrometer's tunable local oscillators were set for simultaneous measurement of two different lines in the upper (USB) and lower (LSB) sidebands. Toward the Galactic center continuum peak (position A), the H42α recombination line in the LSB was combined with the HCN ($J = 1 \rightarrow 0$) transition at 88.632 GHz in the USB. The position B observations of the HCN 1–0 line (LSB) was complemented by a search for the heavy symmetric top molecule CH_3CN ($J = 5 \rightarrow 4$, 91.87 GHz, USB). No emission from CH_3CN greater than 0.2 K brightness temperature was detected. The H42α and 88 GHz radio continuum results will be discussed separately (Wright *et al.* 1986). The correlator bands were partially overlapping to guarantee a total velocity coverage of ≈ 400 km s^{-1} for each line.

Comparison with single-dish HCN spectra, taken in 1986 May with the IRAM 30 m dish (27″ beam) shows that—excepting the spatially extended +20 and +40 km s^{-1} cloud emission—most of the flux toward the inner disk is detected with the interferometer. Farther out ($R \approx 4$ pc), about half of the emission is resolved out. The line profiles of the ring feature are similar in both single-dish and interferometer data sets.

A spectrum of the CO $J = 7 \rightarrow 6$ line toward the position R.A. = $17^h42^m27^s.0$, decl. = $-29°01'03''$ (1950), about 110″ southwest of Sgr A* at position angle about 15° (we follow the convention for position angle ϕ, measured east from north, north at $\phi = 0$) was taken in 1986 June on the 3.8 m UKIRT telescope on Mauna Kea with the UCB/SSL submillimeter heterodyne spectrometer (Harris, Jaffe, and Genzel 1986). The FWHM beam size was about 25″, and the main beam efficiency was about 0.4. The backend spectrometer was an acousto-optical spectrometer with a bandwidth of 600 MHz.

III. RESULTS

Figures 1 through 4 show the basic data. Figure 1 is a relief representation of the velocity integrated HCN map in field A, constructed with the MEM algorithm (5″–7″ resolution). Figure 2 gives a velocity averaged CLEAN map (10″ resolution) combined from the observations in both fields, together with selected spectra. Figure 3 shows (*a*) the velocity-averaged MEM map, superposed on the 5 GHz continuum map by Lo and Claussen (1983), (*b*) the C^+ 158 μm map by Lugten *et al.* (1986) and (*c*) a map of 2.6 mm CO $1 \rightarrow 0$ emis-

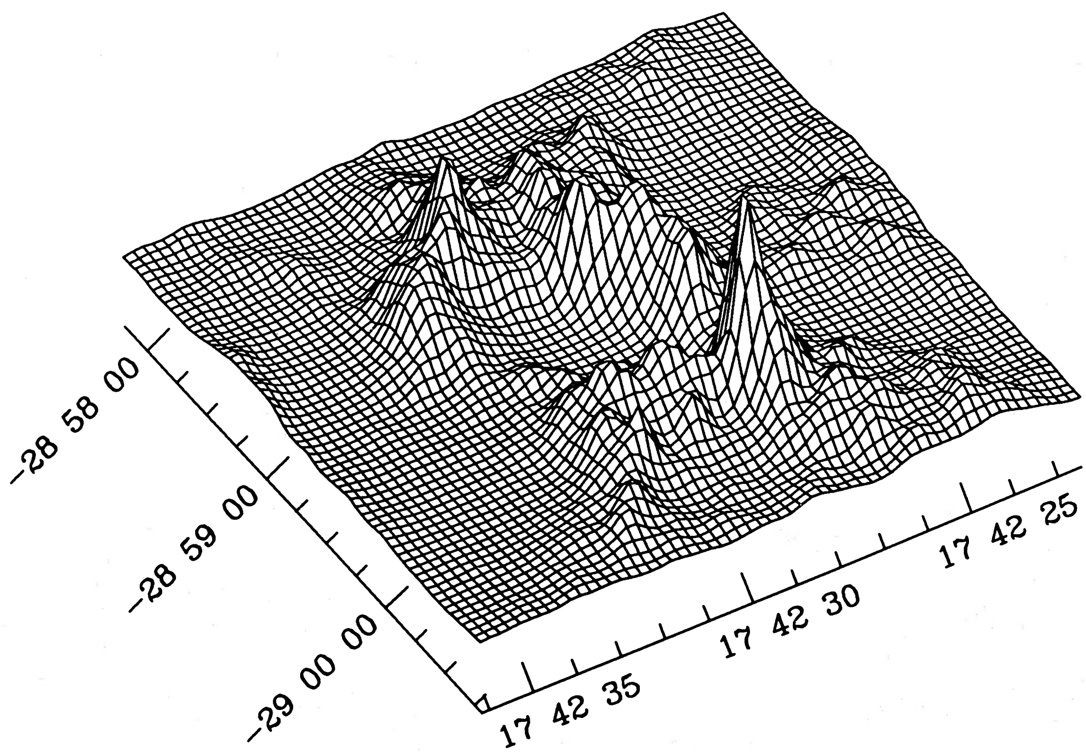

FIG. 1.—Relief representation of the velocity-integrated ($-150 \leq v_{LSR} \leq +150$ km s^{-1}) HCN maximum entropy method (MEM) map (88.632 GHz), centered on the position of Sgr A* (position A). The continuum emission has been subtracted from the map. Spatial resolution is about 5″–7″. The map maximum corresponds to a peak brightness temperature 1.2 K averaged over 300 km s^{-1}. The map is not corrected for the telescope's beam response which has a FWHM of 2′.3.

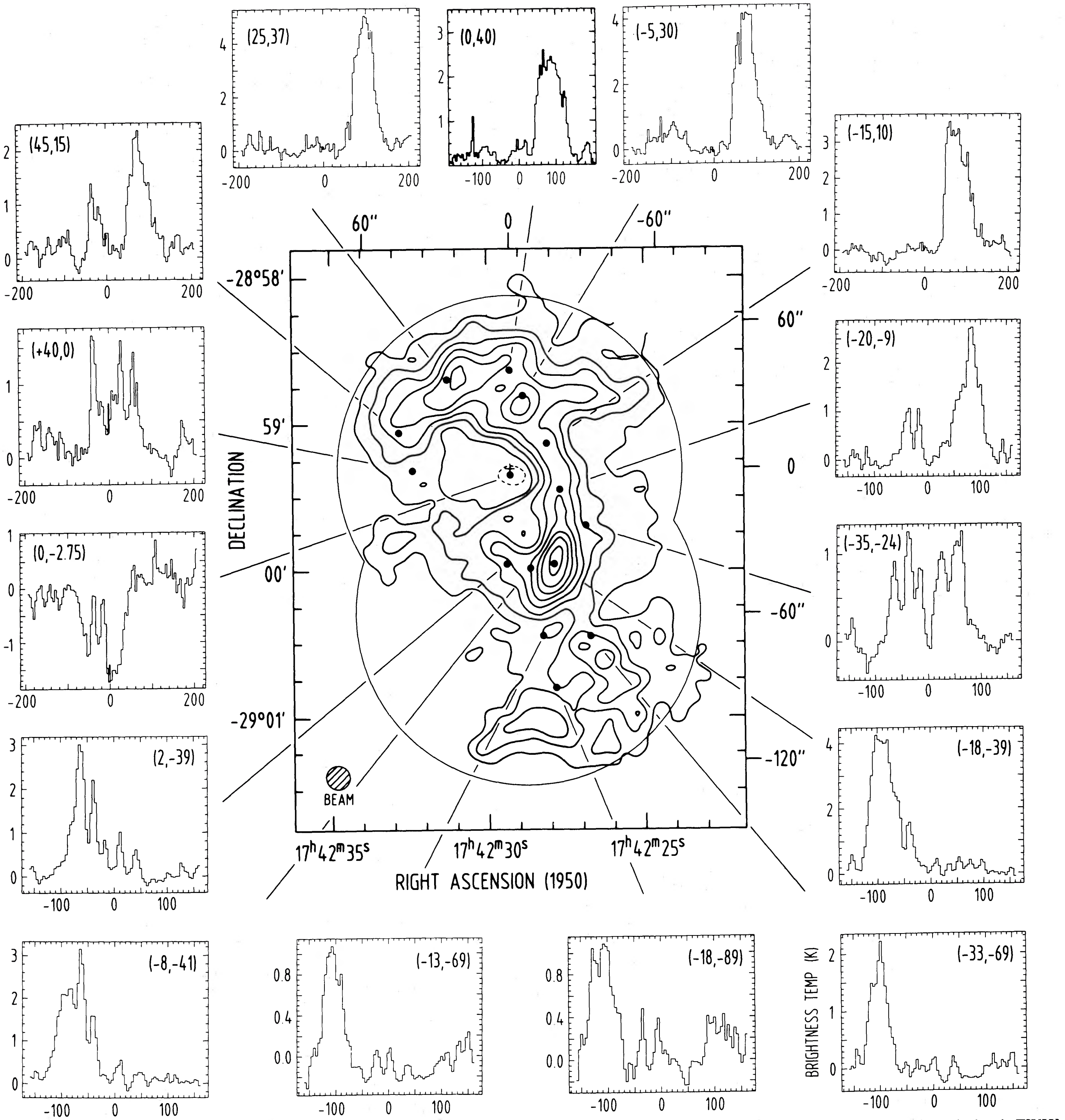

FIG. 2.—CLEAN map of the velocity-integrated ($-150 \le v_{LSR} \le +150$ km s^{-1}) HCN emission, together with typical spectra. The spatial resolution is FWHM 10″.8 × 9″ (R.A. × decl.) for natural weighting of the data; the spectral resolution is 4.23 km s^{-1}. The contour map shown is a composite of the position A and B observations after subtraction of the radio continuum. Neither the maps nor the spectra are corrected for the primary beam response, whose FWHM diameters are indicated by thin circles. The contour interval on the map is 0.16 K averaged over 300 km s^{-1}, and the brightness temperature scale is given adjacent to each spectrum. Note the narrow absorption features due to foreground clouds at $v_{LSR} = -55, -30, 0,$ and $+45$ km s^{-1}.

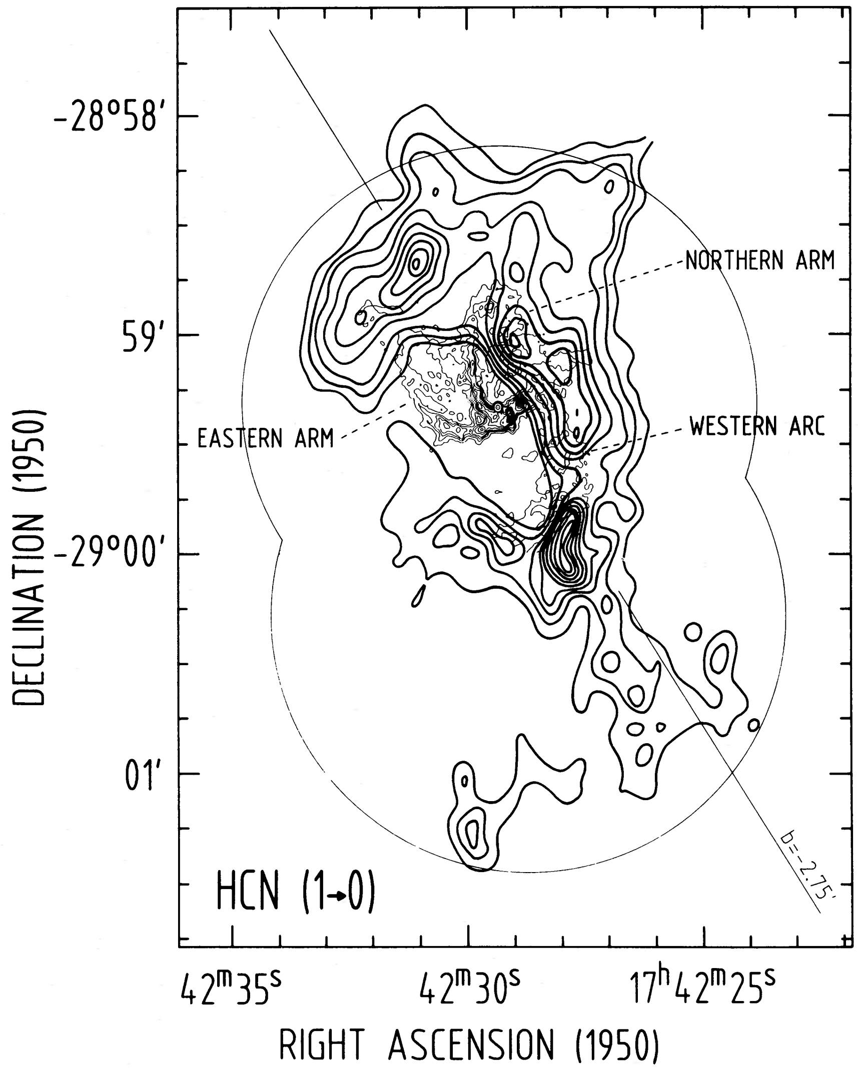

FIG. 3a

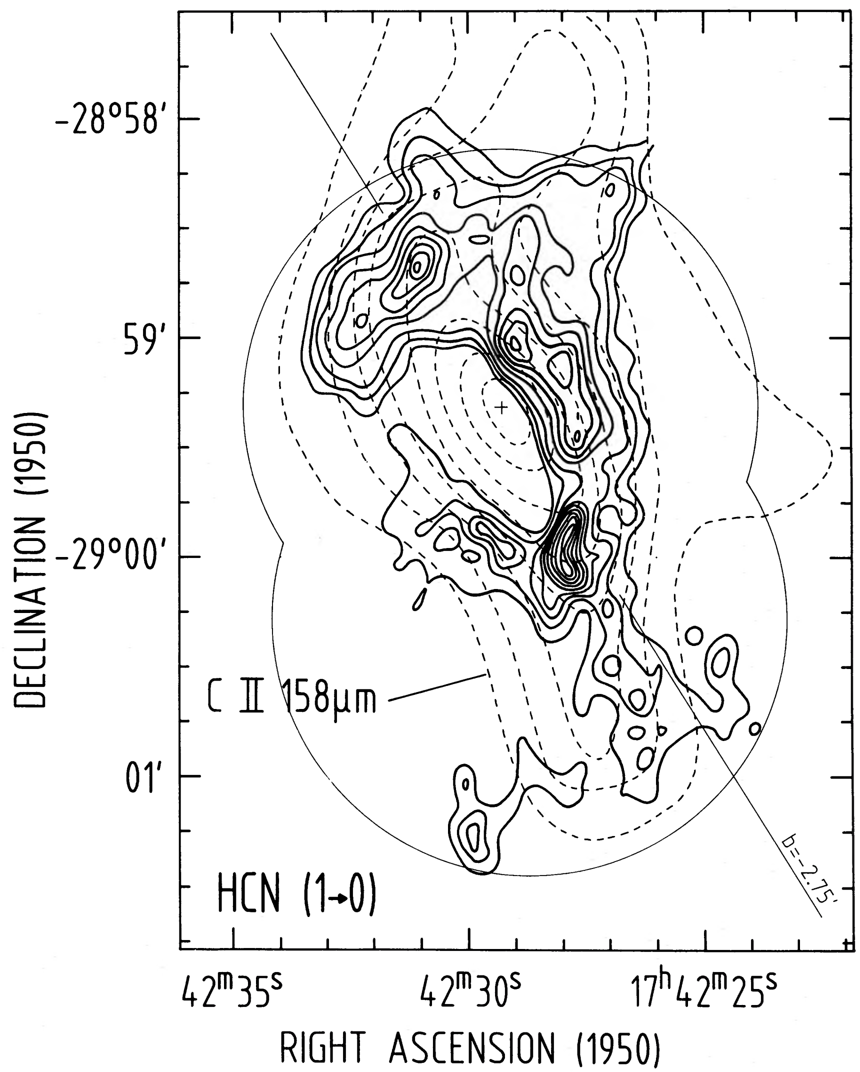

FIG. 3b

FIG. 3.—(*a*) Superposition of the 5 GHz radio continuum map by Lo and Claussen (1983, resolution 1″.0 × 1″.3: *thin contours*) on the velocity-integrated, composite HCN MEM map. The contour interval is 0.12 K averaged over 300 km s^{-1}. The thin, diagonal line marks the direction of the Galactic plane at latitude $b = -2'.75$. The two large thin circles mark the primary FWHM beam diameter of the position A and B observations. (*b*) Superposition of the velocity-integrated HCN MEM map (same as in [*a*]) on the $J = 3/2 \rightarrow 1/2$ [C II] fine-structure line emission ($\lambda = 157.7\ \mu$m) by Lugten *et al.* (1986, effective beam size ≈ 40″–50″; *dashed contours*). A cross marks the position of Sgr A*. Note that the [C II] map is velocity-integrated between −150 and +150 km s^{-1} and has been analyzed with the maximum entropy method. (*c*) Superposition of the HCN map (same as in [*a*]) on the map of CO 1 → 0 emission at $80 \leq |v_{LSR}| \leq 110$ km s^{-1} by Serabyn *et al.* (1986, 21″ beam; *dashed contours*).

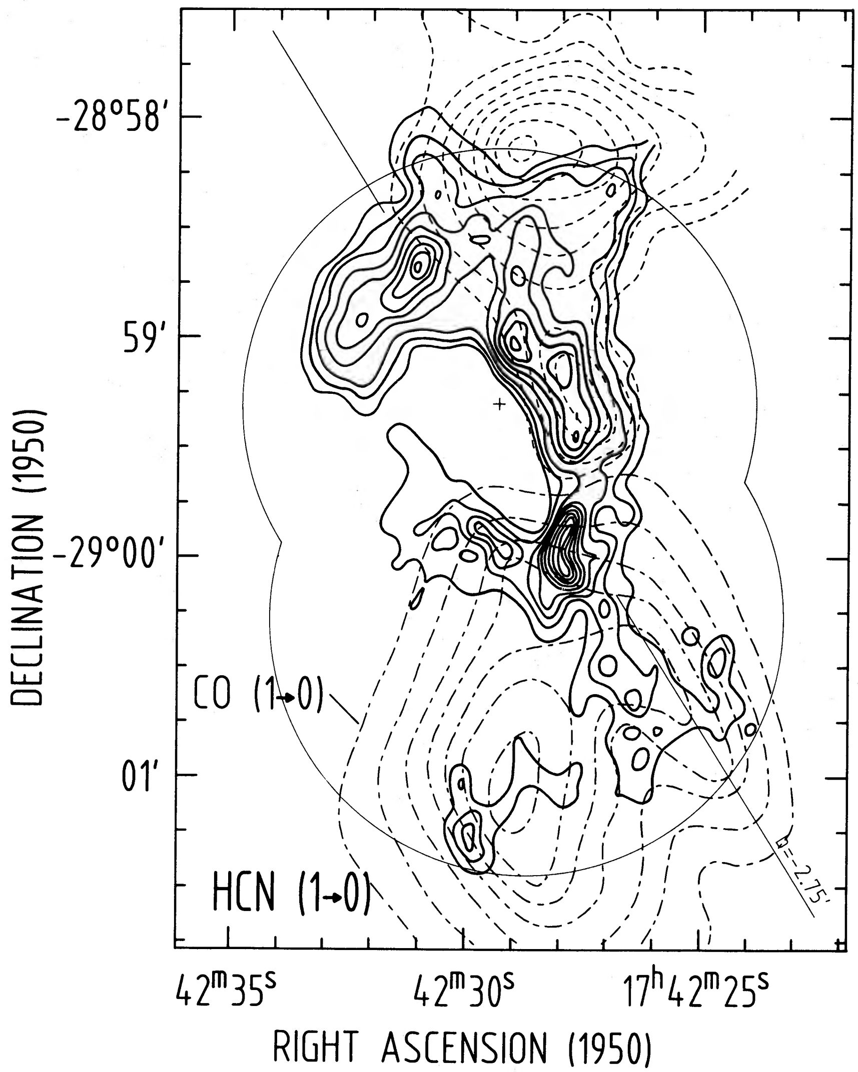

FIG. 3*c*

sion at $80 \leq |v_{LSR}| \leq 110$ km s^{-1} by Serabyn *et al.* (1986). Figure 4 contains representative clean maps of individual velocity channels. The CO $7 \rightarrow 6$ spectrum, along with a single-dish HCN spectrum from the 30 m telescope, a CO $1 \rightarrow 0$ spectrum by Serabyn *et al.* (1986) and a [C II] 158 μm spectrum by Lugten *et al.* (1986), all taken within 10″ of the above position, are shown in Figure 8.

a) *Spatial Distribution*

The velocity-integrated HCN map (Figs. 1 and 2) shows a complete ring of molecular gas surrounding the galactic center. The major and minor axis diameters are about 95″ and 50″ (4.8 and 2.5 pc), with the position angle of the major axis ~30° east of north, that is, approximately along the Galactic plane (position angle 32°). The inferred average inclination is about 60° for an intrinsically circular structure. The center of the ring is offset about 8″ southeast of IRS 16 and the compact radio source Sgr A*. Its inner edge is sharp, with little emission in the inner cavity. The ring appears to be the inner edge of an extended, continuous emission region (a disk) of lower HCN brightness. Our interferometric maps are in good agreement with recent single-dish data from the Nobeyama 40 m millimeter telescope (resolution ~17″) in transitions of ^{13}CO, CS, HCN, and HCO$^+$ (Kaifu *et al.* 1987). In the southwestern part covered by the position 'B' observations, HCN emission can be traced to a radius of ≈100″ (5 pc; Fig. 2). In addition, single-dish HCN, CO, C$^+$, and 0° measurements (Güsten *et al.* 1987; Serabyn *et al.* 1986; Lugten *et al.* 1986; Genzel *et al.* 1985) show emission out to at least 7 pc.

The ring is very clumpy. Most of the brighter clumps in the individual channel maps (Fig. 4) are marginally resolved on the 10″ resolution naturally weighted maps and are clearly resolved on the ~5″ resolution MEM maps. Typical FWHM sizes of individual clumps are about 10″ (0.5 pc), with peak brightness temperatures of the HCN line of 5–10 K. A value of 10″ to 15″ (0.5–0.75 pc) derived from the width of the ring on the maps, represents an upper limit to the thickness of the disk structure at its inner edge.

The molecular ring completely surrounds the center and is a more or less coherent dynamical structure. Although the HCN intensities are weak on the eastern side of the ring, emission at the expected velocities (see § III*e*) is clearly present there. The intrinsic HCN emissivity per volume element near the minor axis on the eastern side of the ring may even be comparable to

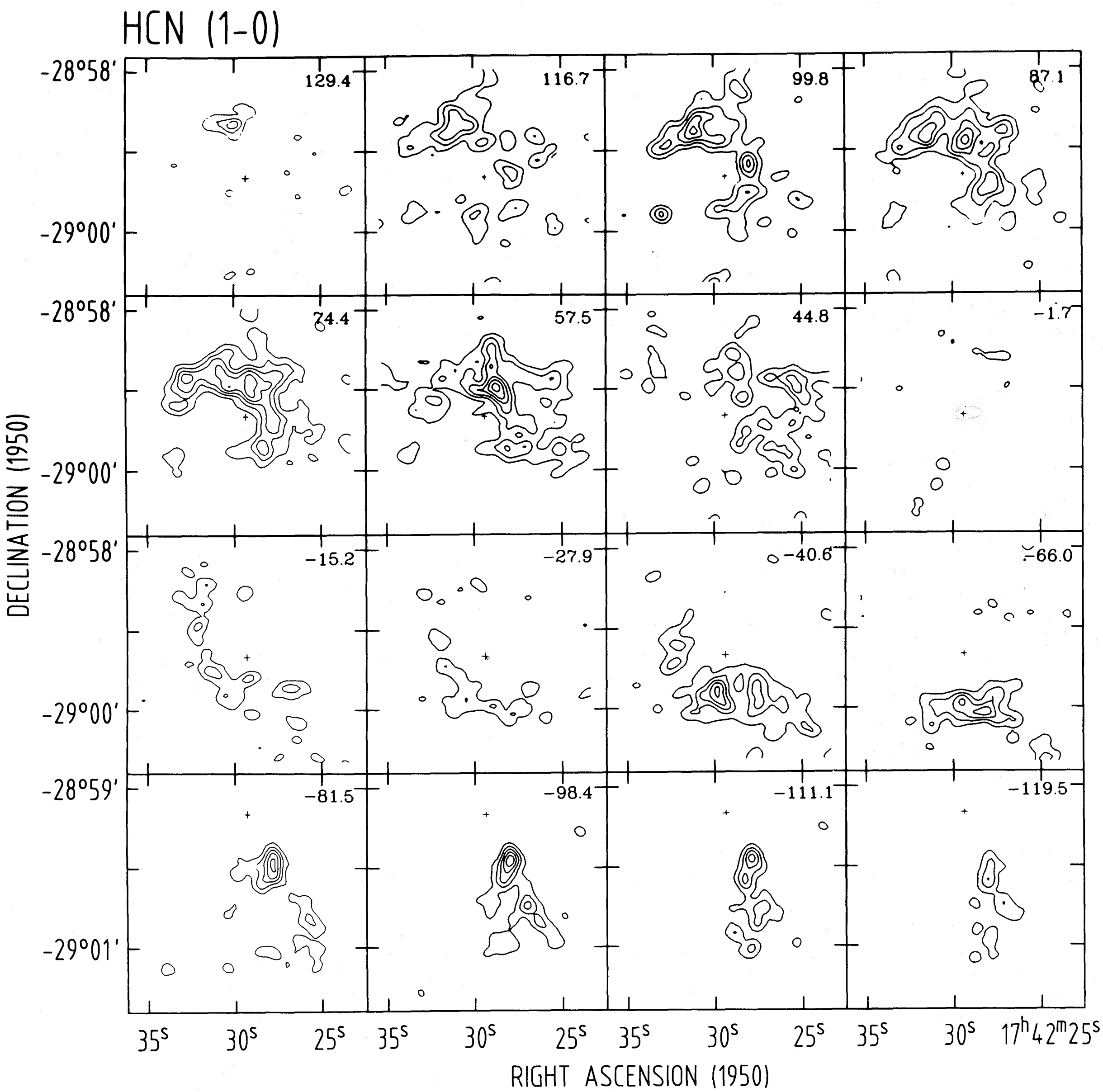

FIG. 4.—CLEAN maps of selected individual velocity channels. Resolution is 10″.8 × 9″ (R.A. × decl.), and the LSR velocity is given for each line channel map. The contour interval is 1 K in brightness temperature. The maps in the upper three rows were constructed from position A; the maps in the fourth row from the top, from position B observations. Note the shift in the map center position in the fourth row. The cross marks the position of Sgr A*.

that near the major axis. The HCN emission near zero LSR velocity is affected by absorption due to cold, foreground clouds. The spectrum toward the continuum peak (Fig. 2) shows three narrow absorption features of moderate optical depth ($\tau \approx 0.2$–0.7) corresponding to well-known extended cloud complexes at 0 km s^{-1} ("local" gas), -30 km s^{-1}, and -55 km s^{-1} (the "3 kpc arm"). The same features are also apparent elsewhere in the HCN spectra of Figure 2 as sharp, deep self-absorption notches. The self-absorption most affects emission near the minor axis of the ring and may absorb up to 50% of the total flux there. With a correction for this absorption, the ratio of line brightness near the major axis to that near the minor axis on the eastern side is about 3 or 4 to 1, consistent with the theoretical ratio in a constant brightness, thin ring of inclination 60°–70°, taking into account the finite beam size.

The velocity-integrated intensity distribution is asymmetric in the sense that the western side of the ring is brighter than the eastern side. Most of that difference is due to a bright cloud of approximately constant velocity ($\sim$60–80 km s^{-1} LSR) on the western side (see discussion in § III*e*).

b) Excitation and Optical Depth of the HCN *Line*

The HCN line is collisionally excited. Genzel *et al.* (1985) and Harris *et al.* (1985) infer hydrogen densities of $\sim 10^5$ cm^{-3} and gas temperatures of 150–450 K at the inner edge of neutral gas ring. The critical density for thermal population of the $J = 1$ level of HCN is a few 10^5 cm^{-3}, suggesting that this level is subthermally excited or barely thermally populated. Given the observationally derived and critical densities, the excitation temperature of the HCN transition in the molecular ring may range between 3 and 10 K. Assuming that the observed clumps are fully resolved with no small-scale ($\ll 10''$) substructure, the HCN brightness temperature at the center of each clump is 2–10 K. Hence, the HCN line may be somewhat optically thick, in which case its brightness temperature is a measure of excitation temperature. The lines are too wide to estimate the optical depth from the strength of the two hyperfine components which are shifted by only $+5$ and -7 km s^{-1} relative to the main line. If the HCN line is optically thick but subthermally populated, the distribution of line emission on the sky probably reflects a combination of hydrogen volume and column density variations. With an assumed hydrogen density of $\sim 10^5$ cm^{-3} and HCN abundance of 10^{-8} to 10^{-7}, H_2 column densities in the HCN emitting gas are 10^{22}–10^{23} cm^{-2}. These column densities are of the same order of magnitude as total column densities in the ring estimated from the far-infrared dust continuum opacity and from the fluxes of the submm and far-infrared CO rotational lines. The HCN map may be a good representative of the overall distribution of dense molecular gas.

c) Comparison to Radio Continuum

The molecular gas surrounds the majority of the ionized gas in Sgr A West (Fig. 3*a*), consistent with the picture of a zone of dense neutral gas and dust surrounding an ionized central cavity (Becklin, Gatley, and Werner 1982). The new data clearly show a general physical relation between the ionized and molecular gas components in the ring.

i) *The Western Arc*

The "western arc" of radio continuum emission (Lo and Claussen 1983; Serabyn and Lacy 1985) is bordered on its outer side by a bright ridge of molecular gas (Fig. 3*a*). Everywhere along the western arc's entire 70″ length the molecular emission peak is just outside of the ionized gas peak. Comparison with the 22 GHz radio continuum map by Ishiguro *et al.* (1986) and with the 88 GHz continuum map (Wright *et al.* 1986) shows that this spatial correlation continues to the northeast beyond the southern tip of the western arc. A good example of a direct spatial correlation between molecular and ionized gas is the brightest HCN peak 40″ SW of the center, where there is a strong enhancement in the western arc's radio continuum emission located near the surface of the HCN clump closest to the center. The velocities of ionized and neutral gas near the western arc are also very similar. These findings are in agreement with the idea (Lo and Claussen 1983; Serabyn and Lacy 1985; Genzel *et al.* 1985) that the western arc is the inner, photoionized surface of the dense neutral ring, where it is exposed to UV radiation from the center.

The thickness of the ionized interface and the separation between peak ionized and molecular emission (5″–10″) are consistent with the expected ionization bounded "bright rim." The ionization front between the western arc and molecular ring is most likely weak D-type, since the density contrast between the molecular material and the ionized cavity is high. For this case, the thickness of the ionized bright rim ΔR may be estimated from ionization and recombination equilibrium (cf. Spitzer, 1978) to be

$$\Delta R < \frac{N_{\rm Lyc}}{4\pi R^2 \alpha(T_e)} \left[\frac{2T_e}{T(\mathrm{H_2})n(\mathrm{H_2})}\right]^2 . \quad (1)$$

The number of Lyman-continuum photons $N_{\rm Lyc}$ deduced from the free-free flux density of Sgr A (20–25 Jy: Brown and Johnston 1983; Ekers *et al.* 1983; Mezger and Wink 1986) is about 3 to 5×10^{50} s^{-1}, taking into account ionizing photons which escape along the poles of the gas disk. The solid angle of the disk as seen from the center is $\Omega_d/4\pi \approx 0.15$ and photons emerging toward the poles may be absorbed further out in lower density gas, as has been proposed by Becklin, Gatley, and Werner (1982). $T_e \approx 8000$ K is the electron temperature, $T(\mathrm{H_2}) \approx 300$ K is the neutral gas temperature, $\alpha(T_e) \approx 4 \times 10^{-13}$ cm^3 s^{-1} is the recombination coefficient, and $n(\mathrm{H_2}) \approx 10^5$ cm^{-3} is the density of molecular gas. At R = 1.7 pc equation (1) then implies $\Delta R \leq 0.3$ pc (6″), in agreement with the maps in Figure. 3*a*.

ii) *The Northern and Eastern Arm and the Bar*

Where the "northern arm" emerges from the central cavity, the ring of HCN emission has a sharp bend and forms a bay enveloping the end of the ionized gas streamer (Fig. 3*a*). The end point of the "eastern arm" (or eastern part of the "bar") is close to another small bend in the HCN ring (see also the lower resolution radio continuum maps by Ishiguro *et al.* 1986 and Brown and Johnston 1983). Adjacent to where the western part of the bar emerges from the cavity and crosses the western arc, there is an HCN feature with unusual kinematics (see §§ III*a* and III*e*). The velocity centroids and widths of the [Ne II] line in the northern and eastern arms at positions closest to the apparent interaction point are about the same as the velocities of the molecular gas just beyond. In contrast, the [Ne II] line at the western edge of the bar is blueshifted by about -100 km s^{-1} while the extra feature in HCN is redshifted by $+70$ km s^{-1}.

These facts suggest that the northern and eastern arms and possibly the western part of the bar are physically coupled to the molecular ring. The ionized streamers may be in the same plane as the neutral gas ring. The new HCN data are in agreement with the suggestion (Ekers *et al.* 1983; Lo and Claussen 1983) that molecular cloudlets in the ring, after losing angular momentum by collision, fall toward the center, are ionized as they enter the central cavity (time scale $\approx 10^4$ yr), and are stretched out to long streamers during the fall (time scale a few 10^4 yr). The spatial distributions and velocities of molecular and ionized gas, therefore, suggest that matter is presently accreting toward the center. The inferred accretion rate depends very much on the assumed electron density. For an accretion time through the central cavity of 2×10^4 yr and electron temperature T_{8000} in units of 8000 K, the mass inflow rate deduced from radio free-free flux density is

$$\dot{M}_{\rm H\,II} = 6.3 \times 10^{-3} S_{20}(\nu_{23})^{0.1}(T_{8000})^{0.35}(n_{5000})^{-1}\ M_\odot\ \mathrm{yr}^{-1}\ , \quad (2)$$

where S_{20} is the radio flux density in units of 20 Jy at frequency ν_{23} in units of 23 GHz, and electron density n_{5000} in units of 5000 cm^{-3}. The electron density in the dense clumps of the bar and northern arm, as estimated from radio emission measure or the ratio of [Ne II] to Humphreys α line (H I, $n = 7 \rightarrow 6$), may range between 10^4 and 10^5 cm^{-3} (Lacy *et al.* 1980; Brown, Johnston, and Lo 1981; Serabyn 1985), resulting in an accretion rate of about 10^{-3} $M_\odot$ yr^{-1} (Lo and Claussen 1983). The high-resolution radio continuum measurements emphasize density condensations, however, and the electron density of a substantial fraction of the ionized gas may be substantially lower. Genzel *et al.* (1984) infer an electron density of $8000^{+\infty}_{-5000}$ cm^{-3} from the line ratio of the high-excitation $\lambda\lambda 52$

and 88 μm [O III] lines. Herter *et al.* (1984) derive an electron density of 1800 ± 500 cm^{-3} from the lower excitation 19 and 33 μm [S III] lines. These latter measurements suggest accretion rates on the order of 10^{-2} $M_\odot$ yr^{-1}.

d) *Comparison with Other Lines*

Figure 3*b* is a comparison between the integrated HCN emission and the [C II] 158 μm fine-structure line emission (Lugten *et al.* 1986), and Figure 3*c* compares the HCN map and a map of CO $1 \rightarrow 0$ emission at $80 \leq |v_{LSR}| \leq 110$ km s^{-1} (Serabyn *et al.* 1986). The HCN ring is part of a much larger disk structure mapped out by the C^+ and CO lines. Much of the difference in spatial distribution of C^+/CO $1 \rightarrow 0$ lines and HCN may be the result of the excitation gradient found by Genzel *et al.* (1985) and Harris *et al.* (1985). The HCN line, requiring high densities for excitation, is brightest near the inner edge, while the C^+ and CO $1 \rightarrow 0$ lines emphasize material of lower density located further out. The CO $1 \rightarrow 0$ line, like HCN, clearly shows the bright, redshifted cloud west of the center.

Gatley *et al.* (1986) presented a 18" spatial and 130 km s^{-1} spectral resolution map of the H_2 $S(1)$ quadrupole line emission at 2.2 μm. The H_2 $S(1)$ line samples hot ($T \approx 2000$ K), shock-excited gas, or gas which is excited by a mixture of shocks and UV excitation (Gatley *et al.* 1986). On the scale of the H_2 spatial resolution, the H_2 and HCN maps have the same overall distribution. The velocities are also comparable, with the possible explanation of a general $+40$ km s^{-1} shift of the H_2 emission from other material (Gatley *et al.* 1986). The redshifted cloud west of the center is prominent in H_2 emission. The HCN line arises from warm (≥ 100 K), dense [$n(H_2) \approx 10^5$ cm^{-3}] gas with a total H_2 colum density of 10^{22}–10^{23} cm^{-2}. The column density of hot H_2 is much smaller [$N(H_2) \approx$ a few 10^{17} cm^{-2}: Gatley *et al.* 1984]. The similar appearances of the H_2 and HCN maps, therefore, suggest that the shocked and/or UV-excited regions emitting 2 μm H_2 lines are closely associated with the warm, dense molecular material.

e) *Velocity field of the Molecular Gas*

In this section we discuss the velocity field of the neutral gas ring derived from the behavior of the velocity centroids with azimuthal angle and radius. We estimated HCN velocity centroids by correcting the line profiles qualitatively for self-absorption by the cold foreground clouds mentioned above. This correction is based on the assumption that the absorptions are narrow for $R < 4$ pc and that the ring feature is much wider in velocity. From the comparison of profiles of the HCN line with those of CO $1 \rightarrow 0$, [Ne II], [C II], and CO $7 \rightarrow 6$, we feel that a reliable and consistent velocity centroid can be obtained in this way for $R < 4$ pc, but not for radii much greater (see further discussion in § IV*b*).

i) *The Inner Edge* ($R \approx 2$ pc)

Figure 5 shows the derived velocity centroids of the HCN emission at the inner edge of the molecular ring. The centroids in the southern part of the ring derived from the A and B data sets agree within the uncertainties. Also indicated on Figure 5 are theoretical curves for a rotating ring of inclination 70° and of inclination 50°. In both cases, we assume the position angle of the major axis (tilt on sky) to be $+27°$ east of north, and the observed peak velocity [$= v_{rot} \sin(i)$] to be 100 km s^{-1}. These values for tilt and peak velocity fit the measured points best. The data can be summarized as follows.

First, the majority of the gas in the ring shows the signature of rotation. Gas following a general rotation pattern can be recognized along most of the circumference of the ring (Figs. 2 and 5). The rotation is strongly perturbed, however. The local "turbulent" velocity width is remarkably large ($\Delta v_{FWHM} \approx$

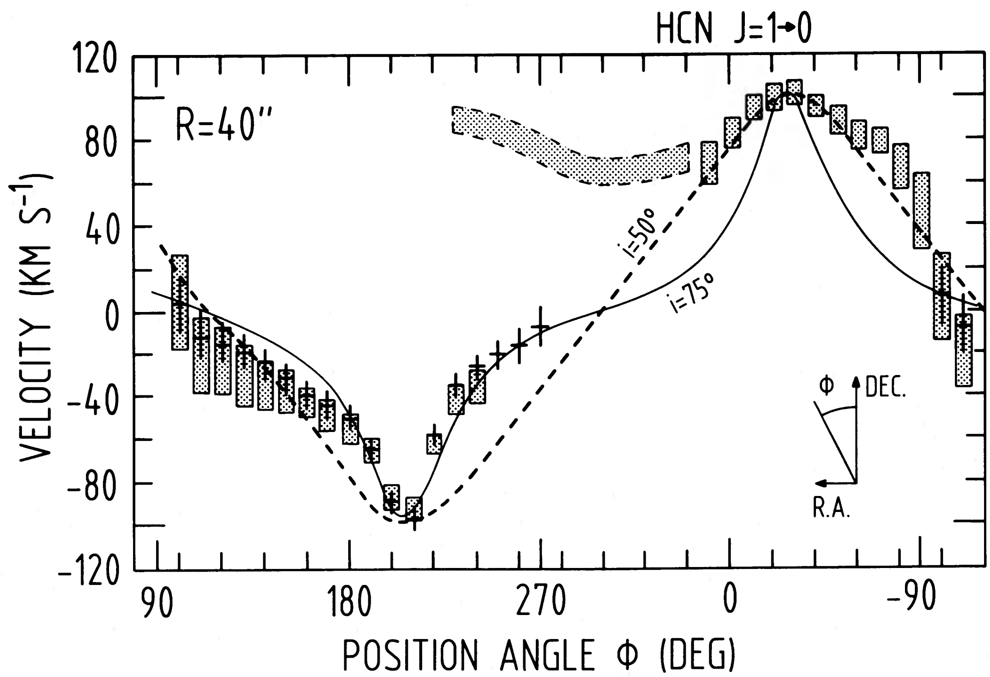

FIG. 5.—Velocity centroids of the 88.6 GHz HCN emission line as a function of position angle on the sky at the inner edge of the Sgr A ring ($R \approx 2$ pc). Data from position A observations are indicated by stippled rectangles; data from position B observations, by crosses. In order to estimate velocity centroids accurately, the original spectra (from naturally weighted, CLEANed data) were qualitatively corrected for absorption features at LSR 0, -30, and -55 km s^{-1} (Fig. 2). Position angle is given in degrees and counted counterclockwise relative to north. Theoretical curves for rotating rings with $v_{rot}/\sin(i) = 100$ km s^{-1}, and position angle 27° east of north, are given for an inclination i of 75° (*thin line*) and 50° (*dashed line*).

50–70 km s^{-1} in a 10″ beam) everywhere in the ring, a significant fraction of the rotation velocity. The ring also appears to be warped. While the southern and western sections of the ring are moderately well fitted by the theoretical pattern of rotation at inclination 70°–75°, the northern and eastern sections require a significantly smaller inclination ($\leq 50°$). The kink or warp inferred from the velocities is also evident in the clearly asymmetric spatial distribution. Figures 3 and 4 show that the apparent ellipticity of the northeastern part of the ring is significantly smaller than that of the southwestern part. Inclinations for the eastern and western parts derived from the ratio of major to minor axes agree well with those derived from the velocities. The kink of the ring may explain the spatial offset between the centroid of the HCN ring and Sgr A*.

Second, there is a bright redshifted cloud northwest of Sgr A* which does not follow the simple circular motion pattern of the rest of the ring. The morphology of the map and the cloud's presence in 2 μm H_2 emission suggest that the cloud is in the Galactic center and located near the ring, but, like the ionized gas in the northern arm, has significant ($\sim$40–80 km s^{-1}) radial velocity. Note that the data *do* show ring material at the proper velocity for rotation along most of the western section.

Third, there is no indication for overall, systematic radial motion of the ring other than by the presence of the cloud just mentioned. A combination of radial and circular motion would manifest itself in a "phase shift" between major axis and maximum velocity axis, that is, in a difference in the position angle of the major axis of the spatial distribution and the position angle where maximum/minimum velocity occurs. Within an uncertainty of $\Delta\phi = \pm 10°$, there is no such shift, limiting overall radial motion to less than $v_{\rm rot} \times \tan \Delta\phi \approx 20$ km s^{-1}. Ellipticity of the overall motion greater than about $\pm 15\%$ along the major axis can also be excluded. Along that direction, the ring appears to be centered within a few arcsec of IRS 16 and Sgr A*, and the observed velocity pattern is symmetric around 0 km s^{-1} LSR.

The major axis at $R \approx 2$ pc is at $\phi = 27° \pm 5°$, which is within 5° of the position angle of the Galactic plane ($\phi_{\rm gp} = +32°$). Correcting the observed peak velocities upward by 3%–7% for inclination and beam smearing (as estimated from numerical modeling) we find a rotation velocity of 109 ± 5 km s^{-1} for the southern and western section and 137 ± 8 km s^{-1} for the northeastern section of the ring. The differences in velocity arises from the difference in inferred inclination.

The predominantly circular motion of the neutral ring at $R \approx 2$ pc (treating the warp as a "small" perturbation) agrees with the ionized gas velocity field in the western arc (Serabyn and Lacy 1985) which also gives a rotation velocity of $\sim$110 km s^{-1}. However, Gatley *et al.* (1986) infer a combination of $\sim$100 km s^{-1} rotation and $\sim$50 km s^{-1} radial motion from the velocities of the H_2 2 μm emission. Since the HCN and H_2 maps are in rather good agreement and probably sample about the same region, the discrepancy lies mainly in the interpretation. Gatley *et al.* (1986) incorporate the "extra" redshifted cloud in their analysis of the ring's motion, resulting in net $\sim$50 km s^{-1} radial motion. We find that rotating gas is present along most of the western section of the ring (Fig. 5) and that the redshifted cloud is an extra feature which is not part of the rotating structure. Radial motion is then not required to explain the velocity field of the ring as a whole.

ii) *The Outer Disk* (2–6 pc)

The present HCN measurements allow us to sample the gas kinematics in the southern (negative velocity) part of the source out to a radius of 4–5 pc. Figure 6 gives the essential characteristics of the velocity field in terms of position-velocity diagrams. Figure 6*a* shows the velocity pattern as a function of position along position angles $\phi = 30°$, corresponding to the major axis of the inner ring, and $\phi = 0°$. Figure 6*b* gives cuts along position angle 100° (approximately along the minor axis of the outer disk) at offsets 10″ and 90″ from the center. The arc structures visible in the two minor axis cuts (*b*-cuts) are signatures of rotation of an inclined disk. For comparison, the insert in Figure 6*b* is a model *b*-cut of a rotating disk of constant brightness, 1.5 pc thickness, rotation velocity 110 km s^{-1}, and inclination 70°. The HCN emission west of the major axis is stronger than east of it (as appears to be the case at the inner edge), but the arc structures otherwise are quite symmetric, thus limiting any radial motion to ≤ 30 km s^{-1}. Serabyn *et al.* (1986) also find no evidence for radial motion greater than 20–30 km s^{-1} from observations of the CO $1 \rightarrow 0$ and CS $2 \rightarrow 1$ lines at 3–7 pc. The asymmetry of the *b*-cuts in the HCN line may indicate an east-west azimuthal density gradient in the disk. The *b*-cuts also contain information on rotation velocity, position angle, inclination, and thickness of the disk at the two radii. The derived quantities as a function of distance from Sgr A*/IRS 16 are plotted in Figure 7.

The observed peak velocity ($\sim$100–105 km s^{-1}) and inferred inclination ($\sim$70–75°) of the HCN emission are approximately constant in the southern part of the ring between 2 to 5 pc from the center. However, the position angle of the axis of peak velocity appears to change with radius. The tilt change is apparent from the position angle of peak velocity in *b*-cuts at different distances from the center. The radial change of the position angle of the major axis is also clearly visible in the "*l*-cuts" of Figure 6*a* which show that the velocity centroids are *decreasing* at position angle $\phi = 30°$ from 2 pc outward, while they are *increasing* along $\phi \approx 0°$. The data on intermediate position angles suggest as well that the position angle of the peak velocity is changing gradually with radius, from about 27° at 2 pc to about 12° at 5 pc. Although the derived tilt change between outer and inner parts of the disk (Fig. 7) is only about 15°, the effect on the velocities is substantial (30%) because of the large inclination. The change in tilt on the sky of the disk's major axis may already be apparent from the spatial distribution of the C^+ emission (see Fig. 3*b*). If the bending of the position angle of peak C^+ and CO emission in the northern part of the ring may also be interpreted as a bending of the disk's major axis, the overall shape is reminiscent of a "trailing spiral." If the Galactic center disk has the characteristics of a trailing dynamical structure, its orientation in space is uniquely determined. Its western edge must be closer to us than its eastern edge, and the western arc would be in front of Sgr A*. Note that this orientation would also be consistent with the curvature of the northern and eastern arms in the central cavity. Liszt *et al.* (1985) find 21 cm H I absorption at $v_{\rm LSR} = 50$–70 km s^{-1} toward and near Sgr A*, consistent with this scenario.

The HCN data clearly show that large turbulent motions are characteristic of the circumnuclear disk out to the largest radii sampled by the present measurements. The velocity dispersion may be decreasing somewhat with distance from the center, from an average of about 55 km s^{-1} at 2 pc to about 37 km s^{-1} at 4–5 pc. Note, however, that the single-dish HCN spectrum at 5.5 pc (Fig. 8) has a width of 56 km s^{-1} which can only in part be accounted for by the large beam size (27″). The local velocity width in the higher excitation CO $7 \rightarrow 6$ and C^+ lines may even be somewhat larger ($\Delta v \approx 70$–80 km s^{-1}). Finally,

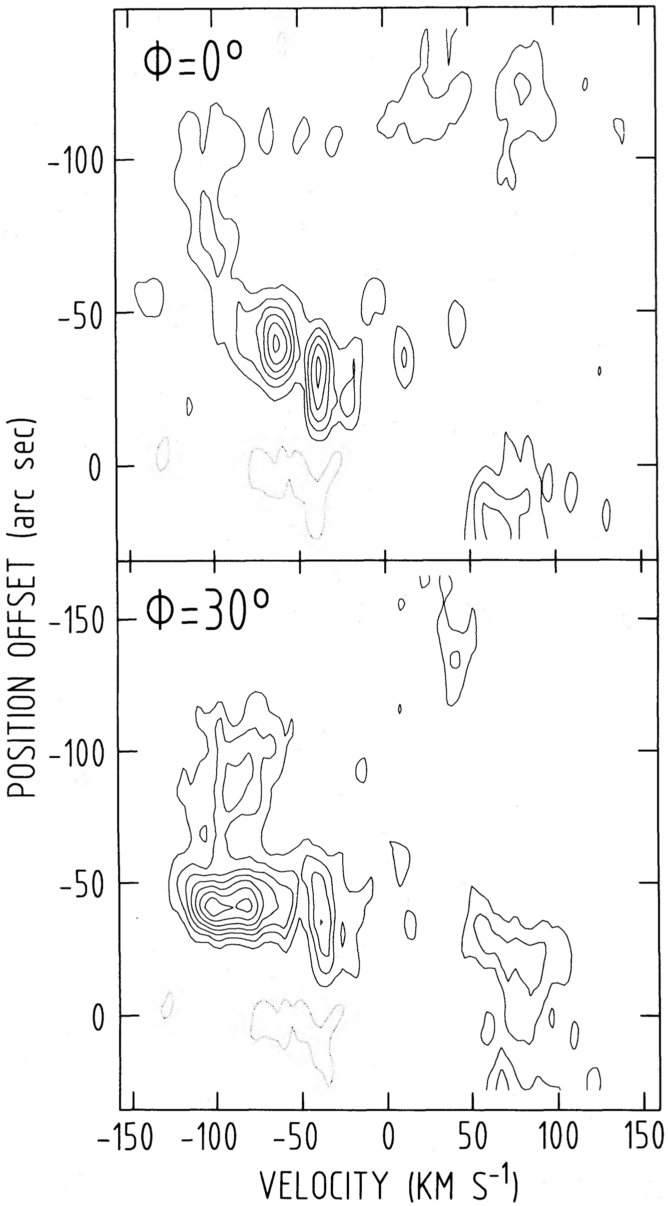

FIG. 6*a*

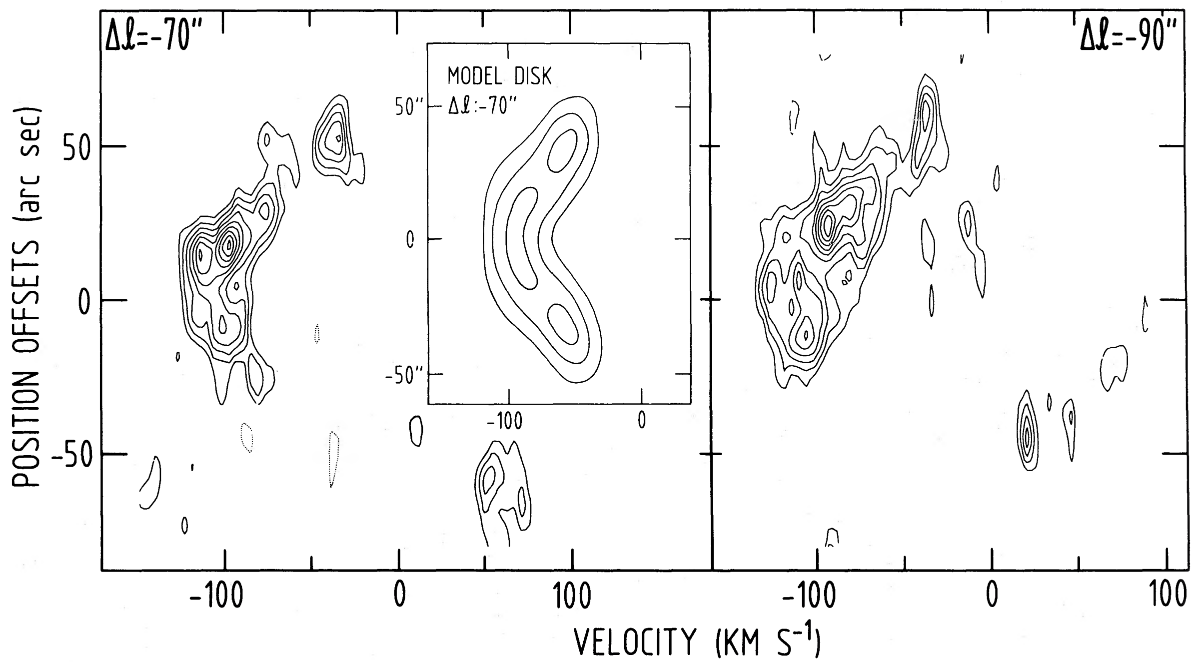

FIG. 6*b*

FIG. 6.—Position-velocity maps of the CLEAN HCN data in the southern part of the ring (position B observations). Spatial resolution is FWHM 10″.8 × 9″ (R.A. × decl.), spectral resolution 4.23 km s^{-1}. (*a*) (*bottom*) Position-velocity map along position angle $\phi = 30°$ toward the southwest relative to the Sgr A* position. Contour unit is 0.5 K. Note the effect of line-of-sight absorption features at −50, −30, and 0 km s^{-1} LSR. (*top*) Position-velocity map along position angle $\phi = 0°$. Contours same as in 6*a* (*bottom*). (*b*) (*top*) Position-velocity map along position angle 100° at on offset −70″ from Sgr A* along the major axis of the disk ($\phi \approx 10°$). Positive offset is toward northwest. The contour unit is 0.2 K. (*bottom*) Position-velocity map along position angle $\phi = 100°$, at an offset of −90″ from Sgr A*. Contours same as in 6(*b*) (*top*). (*insert*) Model *b*-cut of a rotating disk of constant brightness, 1.5 pc FWHM thickness, rotation velocity 110 km s^{-1}, and inclination 72°, for a beam size of 10″ and offset from center of 70″.

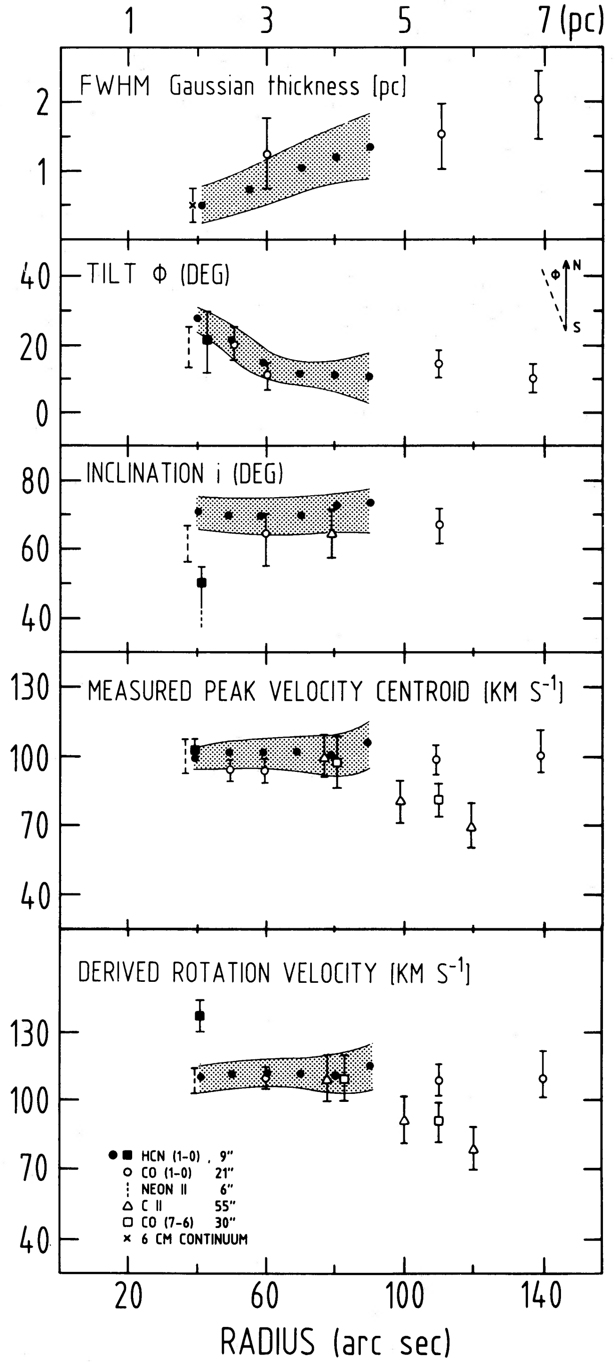

FIG. 7.—Derived parameters of the circumnuclear disk in Sgr A (southern part) as a function of distance from Sgr A*. Small, filled circles and stippled zones represent the 10″ resolution of HCN measurements (this paper); open triangles represent the 50″ resolution [C II] data from Lugten *et al.* (1986); small open circles, the 21″ resolution $J = 1 \rightarrow 0$ CO data by Serabyn *et al.* (1986); the open quadrangle, the 30″ resolution $J = 7 \rightarrow 6$ CO data by Harris *et al.* (1985) and the 25″ resolution CO $7 \rightarrow 6$ data presented in this paper; and the dashed lines, the 6″ [Ne II] data by Serabyn and Lacy (1985). The filled rectangle gives the HCN data point in the northern part of the disk at 2 pc (this paper). Note that the error bars shown are estimates of the *absolute* uncertainties. The uncertainties in relative values are somewhat smaller. From top to bottom the parameters are measured FWHM thickness of the disk, measured position angle of peak velocity on the sky, inferred inclination of disk, measured peak velocity in km s^{-1}, approximately equivalent to $v_{\rm rot}/\sin(i)$, inferred rotation velocity $v_{\rm rot}$ (peak velocity corrected for inclination and beam smearing).

the thickness of the HCN disk, as inferred from the spatial extent at the highest velocity in the *b*-cuts, increases steadily with radius, from about 0.5 pc at 2 pc to 1.4 pc at 5 pc.

IV. DISCUSSION

The new aperture synthesis data establish the existence of a thin, clumpy, and highly inclined circumnuclear ring representing the inner edge of a more extended disklike structure centered near Sgr A*. This molecular disk shows a well-defined central hole and appears to be dynamically coupled to the ionized gas. For most of the molecular gas, rotation around the center is the dominant large-scale motion. The results thus confirm and put on sound foundation earlier analyses of the kinematics and spatial distribution of the neutral interstellar matter in the central 5 pc of the Galaxy (see references in § I).

The HCN data also give a number of surprises. First, the inner rim of the molecular gas is sharp and the distribution is clumpy even though local velocity dispersion in individual clumps is remarkably high throughout the disk. Hence, the appearance of the molecular disk as we observe it today is short-lived and cannot be a static equilibrium configuration. A similar conclusion has been drawn for the ionized gas in the central cavity (Lacy, Townes, and Hollenbach 1982; Lo and Claussen 1983). Second, the data present strong evidence for a change of inclination of the disk at its inner perimeter as well as a change of its tilt angle with radius. The characteristics are interesting on their own as dynamical effects, but they also have important consequences for the interpretation of the velocity field in terms of a rotation curve. We will now discuss these new points in turn.

a) Dynamical Effects in the Ring

Static Equilibrium.—The material in the neutral ring is subject to tidal disruption (clump density $\ll n_{\rm Roche} \approx 10^7$ cm^{-3} at $R = 2$ pc), strong differential rotation, and supersonic collisions between individual clumps. In static equilibrium, one would expect the material to be smeared out with little density contrast over the perimeter of the ring. A single spherical clump of diameter d is stretched by the differential rotation to a filament of length $\approx 2\pi d$ in one rotation period ($\sim 10^5$ yr) about the center. The dynamical time for expansion due to the internal velocity dispersion of the HCN clumps is $\sim 10^4$ yr. Collisions between individual clumps occur on a time scale of one to a few 10^4 yr and may lead to accretion of low angular momentum material toward the center and removal of high angular momentum gas to large radii. The streamers of ionized gas trailing from the ring into the center (Lo and Claussen 1983) and the redshifted HCN feature near the western arc may show exactly this effect. Taking the inferred current mass inflow rate of about 10^{-3} to 10^{-2} $M_\odot$ yr^{-1} and a total gaseous mass of about 10^4 $M_\odot$ between 2 and 4 pc (Genzel *et al.* 1985), the dynamical lifetime of the ring against accretion toward the center may be between 10^6 and 10^7 yr. It is clear *that the present state and appearance of the interstellar gas in Sgr A is shortlived* ($\lesssim 10^5$ yr). The ring either must have been recently created or energy, mass, and clumpiness must be continuously replenished.

Dynamic Equilibrium.—The main issue then is whether there is any conceivable *dynamic* equilibrium which can account for the physical conditions in the circumnuclear ring and for the existence of the central cavity.

The total kinetic energy of non circular motions in the disk between 1.7 and 4 pc, as estimated from velocity dispersion and

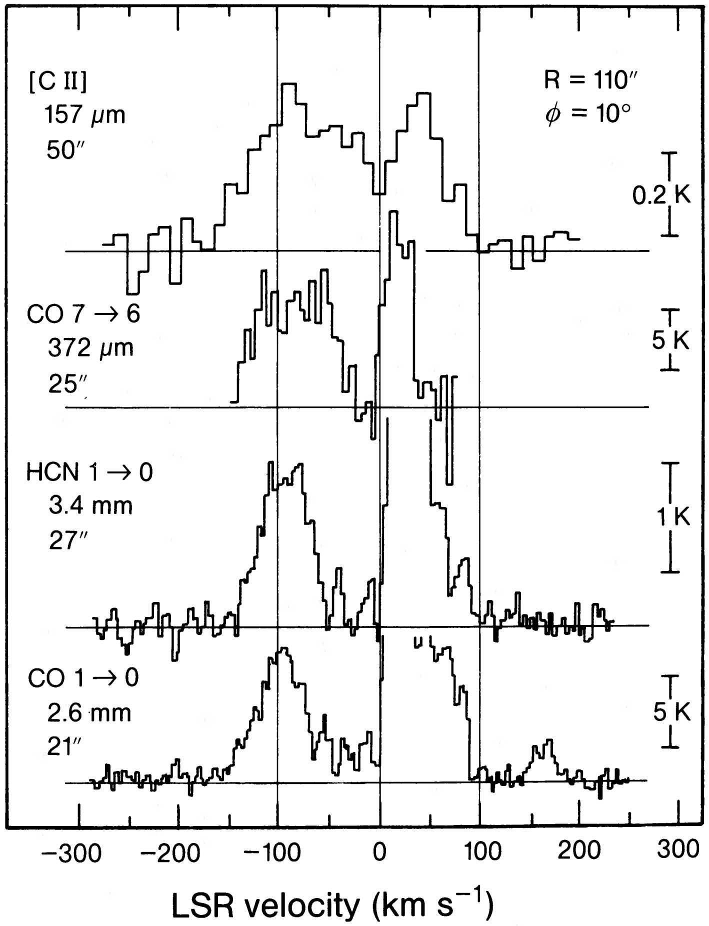

FIG. 8.—Comparison of single-dish spectra of the neutral circumnuclear disk at $R \approx 110''$ from Sgr A*, taken near the position angle of the disk's major axis southwest of the center. From top to bottom, the data are (1) the [C II] $^2P_{3/2} \rightarrow {}^2P_{1/2}$ 157.7 μm line (Lugten *et al.* 1986: Kuiper Airborne Observatory, FWHM 50″ spatial and 35 km s^{-1} spectral resolution with Lorentzian line profile); (2) the CO $J = 7 \rightarrow 6$ 371 μm line (this paper: United Kingdom Infrared Telescope, FWHM 25″ spatial resolution and 5.4 km s^{-1} spectral resolution); (3) the HCN $J = 1 \rightarrow 0$ 3.4 mm line (this paper: 30 m IRAM telescope, 27″ beam, 3.5 km s^{-1} resolution); (4) the CO 1 → 0 2.6 mm line (Serabyn *et al.* 1986: 30 m IRAM telescope, 21″ beam and 2.6 km s^{-1} resolution). Rayleigh-Jeans main-beam brightness temperature scales are given adjacent to the spectra.

gas mass, is about 2×10^{50} ergs. This is a significant fraction ($\sim 15\%$) of the gravitational energy of the gas. The total luminosity of infrared and submillimeter CO, OH, and H_2 line emission from this region is $(1–3) \times 10^4\ L_\odot$. The dissipation rate of the turbulent motions on a collision time scale (2×10^4 yr) is about $7 \times 10^4\ L_\odot$. Hence, intraclump and interclump shocks driven by the supersonic turbulence in the ring offer a natural source of the excitation of the infrared and submillimeter molecular line emission (see discussions in Genzel *et al.* 1985, Harris *et al.* 1985, and Serabyn and Güsten 1986). The measured thickness of the ring is moderately consistent with the turbulence of the gas. For a given rotation velocity $v_{\rm rot}(R)$ at radius R and FWHM turbulent velocity width Δv_t, hydrostatic equilibrium results in a FWHM thickness $\Delta z_{\rm FWHM}$ given by

$$\Delta z_{\rm FWHM} \approx R\, \frac{\Delta v_t}{v_{\rm rot}(R)}\,. \tag{3}$$

The inferred equilibrium width is $\Delta z = 0.85$ pc at $R = 1.7$ pc (for $\Delta v_t = 55$ km s^{-1} and $v_{\rm rot} = 110$ km s^{-1}) and $\Delta z = 1.5$ pc at $R = 4.5$ pc ($\Delta v_t = 37$ km s^{-1} and $v_{\rm rot} = 110$ km s^{-1}), consistent with the measurements at $R > 2$ pc. The thickness at the inner edge is somewhat too small. Note that equation (3) is exact only for a spherically symmetric mass distribution. For a mass distribution which is flattened along the z-axis, Δz differs from the value given in the above equation by a factor smaller than but near unity, depending on eccentricity.

A possible way for continuously replenishing the ring's turbulence and maintaining its thickness may be the dissipation of gravitational energy stored in the differential rotation by "turbulent viscosity" or magnetic stresses (von Weizsäcker 1948; Shakura and Sunyaev 1973; Fleck 1981). The circumnuclear ring/disk in Sgr A may feed interstellar gas into the Galactic center. To account for the observed dissipation rate L_t at 2–4 pc (a few $10^4\ L_\odot$) by conversion of gravitational energy at radius R the mass inflow rate has to be

$$\dot{M}_{\rm in} = \frac{L_t R}{\eta G M(R)} = \frac{L_t}{\eta [v_{\rm rot}(R)]^2}\,. \tag{4}$$

$M(R)$ is the mass contained within R and $\eta \leq 1$ is an efficiency factor. For $L_t = 5 \times 10^4\, L_\odot$, $\eta = 0.5$, and $v_{\rm rot} = 110$ km s^{-1}, the necessary inflow rate is about $5 \times 10^{-2}\ M_\odot$ yr^{-1}. Given that accretion rate, thickness $\Delta z_{\rm FWHM}$ and mean density of hydrogen nuclei $\langle n_{\rm H} \rangle$ of the ring ($\langle n_{\rm H} \rangle \approx$ one to a few 10^4 cm^{-3}; Genzel *et al.* 1985), conservation of mass requires an accretion velocity v_R of about 10–20 km s^{-1} at $R \approx 2$ pc. This is marginally within the observational constraints. The picture of an overall smooth contraction of the ring may also not be completely applicable, since the gas is so clumpy. The accretion may be dominated by sporadic infall of individual, massive streamers at large velocities.

It is not clear whether such an accretion flow fits in with current theoretical ideas (cf. Pringle 1981 for a summary), mainly because of the basic uncertainty in the mechanism and magnitude of viscosity. In the standard α-disk formulation, the expected inflow velocity due to turbulent viscosity of eddies of size $l \approx \Delta z$ and velocity dispersion $\sigma_t = \Delta v_t/2.35$, or due to magnetic stresses is given by

$$v_R = \frac{3}{2}\,\alpha\left(\frac{\Delta z}{R}\right)c_s = \frac{3}{2}\,\alpha\left[\frac{\sigma_t}{v_{\rm rot}(R)}\right]c_s\,, \tag{5}$$

where $c_s \approx 1$ km s^{-1} is the sound speed of the gas. The dimensionless number α is given in Shakura and Sunyaev (1973) as

$$\alpha = \sigma_t/c_s + (v_A/c_s)^2\,, \tag{6}$$

where $v_A \approx 5$ to 10 km s^{-1} is the Alfvén speed.

Turbulence is theoretically expected in accretion disks. Clumpiness might be generated by Rayleigh-Taylor or Parker (Pustilnik and Shvartsman 1974) instabilities. However, the calculations assume subsonic turbulent and inflow velocities. In the Galactic center disk, the measured turbulent velocity ($\sigma_t \approx 23$ km s^{-1} at $R = 2$ pc) and required inflow velocity are supersonic and possibly super-Alfvénic. If the α-disk formulation could be extended to the supersonic case, application of equations (5) and (6) with measured values for σ_t and $v_{\rm rot}$ ($\alpha \approx 20$–100) does indeed result in $v_R \approx 5$–30 km s^{-1}, as expected.

Hence, the turbulent velocity field, the line emission, and possibly the clumpiness of the Galactic center disk may be understandable in the framework of a steady contraction of the disk if the mass inflow rate toward the nucleus is a few 10^{-2} $M_\odot$ yr^{-1}. The accretion disk model is particularly attractive since it could account for the turbulent motions throughout the disk. The large required accretion rate is marginally consistent with the accretion rate of ionized gas at $R < 2$ pc, if much of the ionized gas is at relatively low density ($n < 2000$ cm^{-3}; see discussion in § IIIc).

A Recent Explosion from the Center?—If the amount and dissipation of turbulence in the circumnuclear disk cannot be explained by a large, steady accretion flow from farther out, a recent energetic event is required. Furthermore, the sharp inner edge of the disk and the presence of the central cavity cannot be explained by dynamic equilibrium. The main problem is that there is no obvious mechanism which can balance the large ram pressure ($\sim 10^{-6}$ to 10^{-7} ergs cm^{-3}) and energy density of the turbulent motions at the inner edge of the disk. All conceivable counter pressures fail by one to three orders of magnitude. The radiation pressure of the central source(s) is 3×10^{-9} ergs cm^{-3} (for $L \approx 10^7$ $L_\odot$). The average thermal pressure of the Sgr A H II region is 5×10^{-10} ergs cm^{-3}. The ram pressure of the possible mass outflow from the center inferred by Geballe *et al.* (1984) is 9×10^{-9} ergs cm^{-3} for an outflow rate of 10^{-3} $M_\odot$ yr^{-1} and outflow velocity of 500 km s^{-1}. The "rocket effect" on neutral clouds evaporating in the center's strong UV field (Spitzer 1978) might accelerate in the remaining parts of the clouds to about the sound speed in the ionized gas (-7 km s^{-1} for $T_e = 8000$ K), but probably cannot account for motions of several tens of km s^{-1}. The rocket acceleration certainly cannot account for the turbulent motions throughout the disk or for the existence of a central cavity over a long time period. Magnetic forces could confine the gas in a ring of $R > 2$ pc only if a strong magnetic field ($B \geq 5$ to 10 mG) is present. A strong field of that magnitude is suggested by the polarization of the 10 μm dust emission in the northern arm (Aitken *et al.* 1986). A dynamical resonance in a nonaxisymmetric gravitational field, such as Lindblad resonance, is a possible explanation (see discussion in Genzel *et al.* 1985) but probably requires larger noncircular velocities than observed.

Maybe the most likely explanations are a recent ($t \leq 10^5$ yr) explosion or a large burst in mass outflow from the center. Because of the small covering angle of the disk as seen from the center ($\Omega_{\rm disk}/4\pi \approx 0.15$), the energy of an explosion has to be at least 10^{51} ergs, and the mass outflow rate has to be at least 0.2 $M_\odot$ yr^{-1} for a flow velocity of 500 km s^{-1} to account for the disturbed velocity field in the disk and to clear out the central 2 pc of interstellar material. The present situation may be a quiescent state in which material from the disk is again slowly accreting toward the center. Important questions are then whether material is accumulating in the central pc, leading to a future star formation event and whether a fraction of the gas is accreting toward a possible central massive black hole. An accretion rate of only $\sim 10^{-5}$ $M_\odot$ y^{-1} onto a 10^6 $M_\odot$ black hole would account for the present UV luminosity of Sgr A.

The warp, the radial change in the position angle and the small thickness at $R \approx 2$ pc of the disk are also indicative of a perturbed and short-lived structure. Perturbation of the gravitational potential of the gas by an external source (the Magellanic Clouds; Hunter and Toomre 1969), interaction with streaming, intergalactic gas (Kahn and Woltjer 1959), and dynamical instabilities in a rotating gas disk (Lynden-Bell 1965) have been proposed as the cause of the warping of the large-scale Galactic disk. Similar explanations may be attractive for the Galactic center. The radial change in the position angle of the disk's major axis is reminiscent of a trailing spiral density wave which could be excited by a nonaxysymmetric perturbation (e.g., a bar) of the center's gravitational field. In addition, because of the short time scales involved, the warped structure—like the ionized streamers and the peculiar redshifted HCN feature—may also simply be the result of a recent perturbation. For example, a collision between two large clouds in the ring a few 10^4 yr ago may have thrown them into a different plane of motion. Within half a rotation period, the clouds would then be drawn by the differential rotation into long streamers, giving the appearance of a warping of the overall structure. The consistency of the spatial and velocity patterns favors the picture of an overall warped disk.

b) Comments on the Rotation Curve in the Galactic Center

One of the most fundamental applications of the gas dynamics in the Galactic center is a determination of the rotation curve. If the velocities of the gas can be interpreted as circular motions or in terms of other well-defined orbits in the center's gravitational field, the mass distribution in the central 10 pc may be derived. This approach has been taken by the Berkeley group, who combined a number of spectroscopic measurements of the ionized and neutral gas motions (see Crawford *et al.* 1985 for a summary). Taken together, these measurements indicate a falloff of velocities with distance from the center out to at least 5 pc and suggest that there is an unusual mass concentration in the central few parsecs. A central point mass of (1–4) × 10^6 $M_\odot$ is required (see also Mezger and Wink 1986). An analysis using the virial theorem leads to essentially the same result. Serabyn *et al.* (1986), Lo (1986), Gatley *et al.* (1986), and Allen and Sanders (1986) have challenged that conclusion both in terms of the data (the velocities of CO and CS mm emission lines at $R > 3$ pc do not fall off with distance from the center: Serabyn *et al.* 1986; Lo 1986), as well as in terms of the basic assumptions (the assumption of circular motions or well defined orbits may not be applicable: Lo 1986; Allen and Sanders 1986).

Combining the new HCN measurements with the previous data on the neutral gasdynamics, we come to the following conclusions:

1. The previous assumption of circular motion (rotation) as the *dominant* large scale motion for the majority of the gas is justified for the neutral gas at $R \geq 2$ pc.

2. The various data sets, incorporating a number of independent spectroscopic measurements are in *essential agreement* for $R \leq 5$ pc. This is apparent from Figure 7.

3. Because of the change of the disk's tilt angle with radius, a derivation of a rotation curve from cuts along constant position angle is not appropriate. In particular, the HCN data indicate that much of the observed falloff of velocity centroids along the galactic plane (Fig. 6*a*; cf. Harris *et al.* 1985 and Lugten *et al.* 1986) may be caused by the changes in geometry of the disk. Similarly, the increase of velocities along the major axis ($\phi \approx 10°$) at larger radii observed by Serabyn *et al.* (1986) (see Fig. 6*a*) may be explained by the tilting and not by a large thickness of the disk.

Measured *peak* velocities as a function of distance from IRS 16/Sgr A* for the various data sets are given in Figure 7 (*second from bottom*) and the inferred rotation velocities (corrected for inclination and beam smearing) are given in Figure 7 (*bottom*). In the framework of a *warped, rotating equilibrium disk*, the HCN measurements and all other recent observations of the neutral gas velocities in the southern part of the disk are best fitted by a constant rotation velocity of 105–115 km s^{-1} between 1.7 and 5 pc. Absorption of emission at $|v_{LSR}| \leq 70$ km s^{-1} by foreground clouds probably does not affect the derived rotation curve very much between 2 and 4 pc. Within $R \approx 4$ pc the CO $1 \to 0$, HCN, and CS data, which are most likely influenced by absorption, give the same result as the [C II], CO $7 \to 6$, and [Ne II] measurements which are almost certainly not affected by absorption. The line shapes in Figure 8 shows that reliable estimates of velocity centroids can only be made by comparison of several different lines. The corresponding mass distribution is a distributed mass with $M \approx 2.8 \times 10^6$ R (pc) $M_\odot$ presumably representing the center's stellar cluster. The mass-to-luminosity ratio of the Galactic center stellar cluster then is ≈ 0.8 $M_\odot | L_\odot$.

The inferred rotation velocity in the northern (redshifted) part of the disk at 1.7 pc, however, due to a larger correction for inclination, is significantly larger ($v_{rot} \approx 137 \pm 8$ km s^{-1}). The reason for this difference is not clear. Possible explanations include noncircular or elliptical motions for some parts of the gas.

The velocity patterns in different lines between 4 and 8 pc are more ambiguous and contradictory and may not fit a constant rotation curve. This is shown in Figure 8 which is a comparison between line profiles at $R = 110''$ (5.5 pc) near position angle $\phi \approx 10°$. The CO $1 \to 0$ (Serabyn *et al.* 1986) single-dish line shows a well-defined peak at -90 to -95 km s^{-1} LSR with little emission at $v_{LSR} \geq -60$ km s^{-1}. This is consistent with a rotation velocity of 100–110 km s^{-1} at that radius as well. The single-dish HCN $J = 1 \to 0$ line, on the other hand, shows a splitting of the line profile in components at -100 and -70 km s^{-1} (R. Güsten, private communication). Finally, the [C II] line, as well as the newly measured CO $7 \to 6$ line profile presented in this paper show strong emission at $v_{LSR} \geq -60$ km s^{-1} and have a velocity centroid of -60 to -80 km s^{-1}. This finding was the basis of the derived falloff of rotational velocity by Lugten *et al.* (1986). It is not clear how to interpret the conflicting information. On one hand, the higher excitation lines ([C II], CO $7 \to 6$) are more likely to sample the material *near* the Galactic center and are much less, if at all, affected by foreground absorption. On the other hand, the CO $7 \to 6$ and [C II] lines may not be an unbiased sample of the velocity profile at $R = 5.5$ pc if there is an excitation gradient in the disk because they are so sensitive to excitation. We have plotted both sets of data in Figure 7 and conclude that the rotation curve at $R > 4$ pc may be more complex than for R between 2 and 4 pc.

4. The short dynamical lifetime and the warping and tilting of the disk and the possibility of radial motions of $\sim$10–30 km s^{-1} make an accurate determination and unambiguous interpretation of the rotation curve in terms of a detailed mass distribution difficult. The possibility of a nonequilibrium configuration of the gas velocities, in particular, make a straightforward conversion from velocity to mass distribution somewhat problematic.

V. CONCLUSIONS

Aperture synthesis observations with the Hat Creek millimeter wave–interferometer have been used to study the circumnuclear neutral gas ring in the Galactic center at high spatial and spectral resolution. The molecular emission line observed, HCN $J = 1 \to 0$ at 88.6 GHz, samples dense and warm gas at the interface between the ionized central 2 pc and cooler, lower density molecular gas at $R > 5$ pc from the center. In addition, we have taken HCN $1 \to 0$ and CO $7 \to 6$ single-dish line profiles at $R \approx 5.5$ pc to sample the velocity field at larger radii.

The new data demonstrate the existence of a highly inclined thin, and clumpy ring or disk of molecular material centered on IRS 16 and the radio point source. The disk has a well-defined central hole of radius ≈ 1.7 pc. An intimate morphological and dynamical relationship between ionized and molecular gas is present. Perturbations in the HCN spatial and velocity structure near the streamers of ionized gas indicate an accretion flow toward the Galactic center, in agreement with the proposal by Lo and Claussen (1983). An overall contraction of the disk toward the nucleus may in part feed the large turbulence of the disk.

Given the unusually high local velocity dispersion and the similarity between the HCN map and the map of 2 μm H_2 quadrupole emission by Gatley *et al.* (1986), the most likely excitation mechanism for the 2 μm hydrogen line emission as well as for the CO and OH far-infrared/submillimeter lines may be shocks driven by local turbulence, or a combination of cloud-cloud shocks and mass outflow from the center.

The earlier analysis of the ring's large scale motion in terms of rotation is supported by the HCN data. The rotation, however, appears to be perturbed by a large local velocity dispersion, by warping of the structure, and by at least one cloud probably located in the ring, but not participating in the rotation.

The present spatial distribution and velocity field of the interstellar gas in the central few parsecs (in particular, the central cavity) is not an equilibrium configuration and must have been created or replenished within the last 10^5 yr.

The non-equilibrium situation and complex structure of the gas make a detailed derivation of the mass distribution from the rotation curve more uncertain than previously assumed. In the framework of a warped, rotating equilibrium disk, the HCN measurements and all other recent observations of the neutral gas kinematics in the blueshifted gas south of the center are best consistent with a rotation velocity of 105–115 km s^{-1} between 1.7 and 4 pc. Higher velocities (130–140 km s^{-1}) are indicated by the HCN data in the northern part of the ring at 1.7 pc. Lower velocities (70–80 km s^{-1}) are present in C^+ and CO 7 $\rightarrow$ 6 measurements at distances ≥ 4 pc from the center.

We thank J. Carlstrom, R. Plambeck, J. Welch, and the staff of the Radio Astronomy Lab for their help and support with this program. We are grateful to J. Lugten and C. H. Townes for helpful discussions. R. Güsten thanks the University of California, Berkeley, Physics and Astronomy departments for the hospitality he received during his stay in 1986 winter. This project was supported by NSF grant AST 84-16177 and by the Presidential Young Investigator's Award to R. Genzel (NSF grant 1-444010-21955 and a grant by Rockwell International).

REFERENCES

Aitken, D. K., Roche, P. F., Bailey, J. A., Briggs, G. P., Hough, J. H., and Thomas, J. A. 1986, *M.N.R.A.S.*, **218**, 363.
Allen, D. A., and Sanders, R. H. 1986, *Nature*, **319**, 191.
Becklin, E. E., Gatley, I., and Werner, M. W. 1982, *Ap. J.*, **258**, 135.
Brown, R. L., and Johnston, K. J. 1983, *Ap. J. (Letters)*, **268**, L85.
Brown, R. L., Johnston, K. J., and Lo, K. Y. 1981, *Ap. J.*, **250**, 155.
Crawford, M. K., Genzel, R., Harris, A. I., Jaffe, D. T., Lacy, J. H., Lugten, J. B., Serabyn, E., and Townes, C. H. 1985, *Nature*, **315**, 467.
Ekers, R. D., van Gorkom, J. H., Schwarz, U. J., and Goss, W. M. 1983, *Astr. Ap.*, **122**, 143.
Fleck, R. C. 1981, *Ap. J. (Letters)*, **246**, L151.
Gatley, I., Jones, T. I., Hyland, A. R., Beattie, D. H., and Lee, T. J. 1984, *M.N.R.A.S.*, **210**, 565.
Gatley, I., Jones, T. I., Hyland, A. R., Wade, R., Geballe, T. R., and Krisciunas, K. 1986, preprint.
Geballe, T. R., Krisciunas, K., Lee, T. J., Gatley, I., Wade, R., Duncan, W. D., Garden, R., and Becklin, E. E. 1984, *Ap. J.*, **284**, 118.
Genzel, R., Watson, D. M., Crawford, M. K., and Townes, C. H. 1985, *Ap. J.*, **297**, 766.
Genzel, R., Watson, D. M., Townes, C. H., Dinerstein, H. L., Hollenbach, D., Lester, D. F., Werner, M. W., and Storey, J. W. V. 1984, *Ap. J.*, **276**, 551.
Genzel, R., Watson, D. M., Townes, C. H., Lester, D. F., Dinerstein, H. L., Werner, M. W., and Storey, J. W. V. 1982, in *The Galactic Center*, ed. G. Riegler and R. Blandford (New York: American Institute of Physics), p. 72.
Gull, S. F., and Daniell, G. J. 1978, *Nature*, **272**, 686.
Güsten, R., *et al.* 1987, in preparation.
Harris, A. I., Jaffe, D. T., and Genzel, R. 1986, *Proc. Soc. Photo-Opt. Instr. Eng.*, in press.
Harris, A. I., Jaffe, D. T., Silber, M., and Genzel, R. 1985, *Ap. J. (Letters)*, **294**, L93.
Herter, T., Houck, R. R., Shure, M., Gull, G. E., and Graf, P. 1984, *Ap. J.*, **287**, L15.
Hunter, C., and Toomre, A. 1969, *Ap. J.*, **155**, 747.
Ishiguro, M., *et al.* 1986, preprint.
Kahn, F. D., and Woltjer, L. 1959, *Ap. J.*, **130**, 705.
Kaifu, N., Hayashi, M., Inatani, J., and Gatley, I. 1987, in *Proc. "Galactic Center" Symposium in Honor of Charles H. Townes*, ed. D. Backer (New York: AIP), in press.
Lacy, J. H., Townes, C. H., Geballe, T. R., and Hollenbach, D. J. 1980, *Ap. J.*, **241**, 132.
Lacy, J. H., Townes, C. H., and Hollenbach, D. J. 1982, *Ap. J.*, **262**, 120.
Lester, D. F., Werner, M. W., Storey, J. W. V., Watson, D. M., and Townes, C. H. 1981, *Ap. J. (Letters)*, **248**, L109.
Liszt, H. S., Burton, W. B., and van der Hulst, J. M. 1985, *Astr. Ap.*, **142**, 237.
Liszt, H. S., van de Hulst, J. M., Burton, W. B., and Ondrechen, M. P. 1983, *Astr. Ap.*, **126**, 341.
Lo, K. Y., 1986, *Science*, in press.
Lo, K. Y., and Claussen, M. J. 1983, *Nature*, **306**, 647.
Lugten, J. B., Genzel, R., Crawford, M. K., and Townes, C. H. 1986, *Ap. J.*, **306**, 691.
Lynden-Bell, D. 1965, *M.N.R.A.S.*, **116**, 443.
Mezger, P. G., and Wink, J. E., 1986, *Astr. Ap.*, **157**, 252.
Pringle, J. E. 1981, *Ann. Rev. Astr. Ap.*, **19**, 137.
Pustilnik, L. A., and Shvartsman, V. F. 1974, in *Gravitational Radiation and Gravitational Collapse*, ed. C. de Witt-Morelle (Dordrecht: Reidel), p. 213.
Serabyn, E. 1985, Ph.D. thesis, University of California, Berkeley.
Serabyn, E., and Güsten, R. 1986, *Astr. Ap.*, **161**, 334.
Serabyn, E., Güsten, R., Wink, J. E., Walmsley, C. M., and Zylka, R. 1986, *Astr. Ap.*, submitted.
Serabyn, E., and Lacy, J. H. 1985, *Ap. J.*, **293**, 445.
Shakura, N. I., and Sunyaev, R. A. 1973, *Astr. Ap.*, **24**, 337.
Spitzer, L., Jr. 1978, *Physical Processes in the Interstellar Medium* (New York: Wiley and Sons), chaps. 5 and 12.
Ulich, B. L. 1981, *A.J.*, **86**, 1619.
von Weizsäcker, C. F. 1948, *Naturforsch.*, **3a**, 524.
Welch, W. J., and Thornton, D. D. 1985, in *Proc. International Symposium on Millimeter and Submillimeter Wave Astronomy* (*U.R.S.I.*), ed. J. Gómez-González (Granada: Imprenta Ntra. Sra. de las Angustias), p. 53.
Wright, M. C. H., *et al.* 1986, in preparation.

R. Genzel, A. I. Harris, and J. Stutzki: Max-Planck-Institut für Physik und Astrophysik, Institut für Extraterrestrische Physik, D-8046 Garching bei München, Federal Republic of Germany

R. Güsten: Max-Planck-Institut für Radioastronomie, Auf dem Hügel 69, D-5300 Bonn 1, Federal Republic of Germany

D. T. Jaffe: Department of Astronomy, R. L. Moore Hall, University of Texas, Austin, TX 78712

M. C. H. Wright: Radio Astronomy Laboratory, University of California, Berkeley, CA 94720